AD-A121 115 HGCDTE SURFACE STUDY PROGRAM(U) SANTA BARBARA RESEARCH 1/1
CENTER GOLETA CALIF J A WILSON ET AL. MAR 82
MDA903-80-C-0496

UNCLASSIFIED F/G 7/4 NL

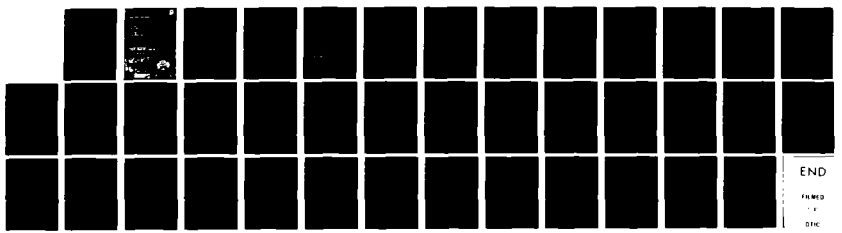

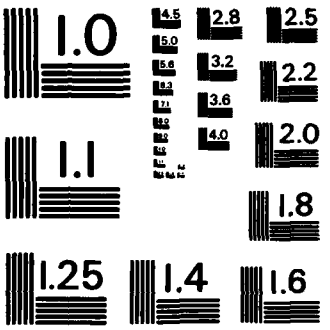

MICROCOPY RESOLUTION TEST CHART
NATIONAL BUREAU OF STANDARDS - 1963 - A

UNCLASSIFIED

SECURITY CLASSIFICATION OF THIS PAGE *(When Data Entered)*

REPORT DOCUMENTATION PAGE		READ INSTRUCTIONS BEFORE COMPLETING FORM
1. REPORT NUMBER	2. GOVT ACCESSION NO. AD-A121115	3. RECIPIENT'S CATALOG NUMBER
4. TITLE *(and Subtitle)* HgCdTe Surface Study Program		5. TYPE OF REPORT & PERIOD COVERED Semiannual Technical Report September 1981 - March 1982
		6. PERFORMING ORG. REPORT NUMBER
7. AUTHOR(s) Jerry A. Wilson, Joel Silberman, Per Morgen and W.E. Spicer		8. CONTRACT OR GRANT NUMBER(s) MDA-903-80-C-0496
9. PERFORMING ORGANIZATION NAME AND ADDRESS SBRC, 75 Coromar Drive, Goleta, CA 93117; Stanford Electronics Laboratories, Stanford, CA 94305		10. PROGRAM ELEMENT, PROJECT, TASK AREA & WORK UNIT NUMBERS
11. CONTROLLING OFFICE NAME AND ADDRESS Defense Advanced Research Project Administration, 1400 Wilson Blvd., Arlington, VA 22209		12. REPORT DATE March 1982
		13. NUMBER OF PAGES
14. MONITORING AGENCY NAME & ADDRESS *(if different from Controlling Office)* Night Vision and Electro-Optics Laboratory, NVEOL-RD, Fort Belvoir, VA 22060		15. SECURITY CLASS. *(of this report)* UNCLASSIFIED
		15a. DECLASSIFICATION/DOWNGRADING SCHEDULE

16. DISTRIBUTION STATEMENT *(of this Report)*

This document has been approved for public release and sale; its distribution is unlimited.

17. DISTRIBUTION STATEMENT *(of the abstract entered in Block 20, if different from Report)*

18. SUPPLEMENTARY NOTES

19. KEY WORDS *(Continue on reverse side if necessary and identify by block number)*

HgCdTe, CdTe, HgTe, photoemission spectroscopy, electronic structure, interface states, DLTS, alloy bonding

20. ABSTRACT *(Continue on reverse side if necessary and identify by block number)*

Electronic structure of the HgCdTe bulk and surface regions as well as passivated interfaces has been studied using a variety of techniques. Capacitance-voltage (C-V) and deep level transient spectroscopy (DLTS) has been used to probe interface states in MIS devices formed with anodic oxides or SiO_2. Ellipsometry was used to monitor the effects of surface treatments. Results indicate the final structure is principally due to prepassivation processing through its effect on surface oxidation. These treatments are seen to effect electronic activity thousands of Angstroms below the interface.

DD FORM 1 JAN 73 1473 EDITION OF 1 NOV 65 IS OBSOLETE

UNCLASSIFIED

SECURITY CLASSIFICATION OF THIS PAGE *(When Data Entered)*

Photoemmission spectroscopy was used to probe bulk band structure and indicates a fundamental difference in bonding of Cd and Hg to the lattice. A breakdown of the virtual crystal approximation is noted and an improved computation for this alloy discussed.

Oxygen chemistry was also studied using PS which indicates that the natural oxide formed on exposure to excited oxygen does not contain Hg. Differences in oxidation between HgCdTe and HgTe indicate Cd plays a key role in the oxidation.

Auger electron spectroscopy coupled with ion sputtering (AES-sputter profiting) has been used to investigate the anodic oxide interface. A small amount of Hg is detected in the oxide while no Hg depletion in the alloy due to anodization is seen.

TABLE OF CONTENTS

TABLES

ILLUSTRATIONS

SUMMARY

This report presents progress of the HgCdTe Surface Study Program (DARPA Contract MDA-903-80-C-0496) during the six month period ending March 1, 1982. During this time experiments were done which focus on the bulk electronic structure of the HgCdTe alloy, the oxygen chemistry of the surface, composition of the anodic axode interface and electronic structure of the passivated interface.

The interface structure has been examined using capacitance-voltage (C-V) and deep level transient spectroscopy (DLTS). Ellipsometry was also used to monitor surface conditions during the prepassivation processing. These results indicate that a very high quality interface can be produced by processing steps which promote the growth of a thin layer of Te-oxide (probably TeO_2) before the application of the passivation (SiO_2). Surface treatments used were seen to effect bulk electronic structure to depths on the order of a thousand Angstroms. The effect is the depletion of the activity of a trap associated with a Hg vacancy complex. The alteration seen at this depth may be a more sensitive measure of the alteration of Hg concentration seen in electro reflectance measurement of the etched surface.

Ion milling and Auger electron spectroscopy (sputter/Auger) have been used to measure the composition of the anodic oxide and interface region on HgCdTe. The oxide consists of Cd and Te oxides with a few percent Hg. The subinterface region shows the same elemental profiles as a processed unanodized wafer. Hg depletion due to anodization was not detected. The oxide formed by exposing the vacuum cleaved surface to excited oxygen has been found to be fundamentally different from the anodic oxide. Here the steps involved in the initial oxygen reaction were resolved as well as measuring the final composition. This was done by controlling the exposure to oxygen and monitoring the changes in bonding by observing line shifts seen in photoemission spectroscopy (PS). This indicates that a Te oxide is produced with some Cd concentrated in the outer layer. No Hg is involved in the oxide. By comparing results from HgCdTe and HgTe, it has been determined that Cd plays a strong role in oxidation of the alloy.

Bulk band structure has been probed with PS which indicates a fundamental difference between Cd and Hg bonding to the lattice. The difference becomes greater and the Hg bond becomes weaker as the Hg concentration increased (lower x). This may have an important connection to the decreased resistance to defect formation of the longer wavelength compositions.

INTRODUCTION

The surface and interface properties of HgCdTe can have a first-order effect on the performance and stability of devices made with this material.

This alloy presents a special problem because one of the alloy components, Hg, is much less strongly bonded than the others. Also, the bonding becomes weaker as Hg content increases. This leads to a number of important effects which impact surface properties.[1-2] The two principal effects of immediate importance are the ease with which defects are induced, principally Hg vacancies and local alternations of stoichiometry.[3] Both have strong effects on electronic structure and oxide formation, which together determined the effectiveness of surface passivation.

Analysis of the electronic structure of the interface and interface region by capacitance-voltage (C-V) and deep level transient spectroscopy (DLTS) shows a strong dependence on surface treatment (particularly oxide growth, as revealed by surface ellipsometry) prior to application of the passivant. This is discussed in detail in Section 1.

Through the use of ultraviolet photoemission spectroscopy (UPS), investigation of the bulk electronic structure of $Hg_{1-x}Cd_xTe$ and its composition dependence produce evidence of differences in the bonding of Hg and Cd in the lattice.[4] Until recently, theoretical treatments of the electronic structure assumed a compositionally weighted average potential for the cations. Results obtained in this work indicated a breakdown of this approximation. The calculation by Chen and Sher,[5] however, used a technique which retains the difference in Cd and Hg potentials. This latter approach successfully predicts the trends observed in our UPS data as the CdTe mole fraction varies. Continuing discussion between the group at Stanford and A. Sher has clarified features of the alloy electronic structure and important and far-reaching ramifications of the difference in Hg and Cd bonds for the materials properties. These topics are discussed in the paper appended to this report. Work is underway to determine the conection between the unusual materials and electronic properties of this alloy.

To explore the oxygen chemistry of the clean surface, cleaved (110) surfaces of CdTe, $Hg_{0.78}Cd_{0.22}Te$, and HgTe were exposed to oxygen excited by an operating ionization gauge. These surfaces were monitored during this process by UPS and X-ray photoemission spectroscopy (XPS). In the alloy and HgTe, an oxide is formed on CdTe and HgCdTe for the exposure conditions used. In addition, the oxygen uptake was greater for the alloy than for HgTe, further indicating the contribution of Cd to the process. The results of this investigation are presented in detail in Section 2.

Auger electron spectroscopy (AES) combined with inert gas ion sputtering (AES-sputter profiling) is a technique well suited to determine the variation with depth of elemental components of systems such as oxidized semiconductors. In the case of HgCdTe, artifacts induced by the sputtering process can make interpretation of the measured profile difficult.[6] Efforts to unravel the true composition profile from the measured one are still in progress. Application of AES-sputter profiling to anodic oxides grown on HgCdTe substrates indicates that the oxide contains only a small concentration of Hg. Mercury depletion of the substrate beyond the oxide semiconductor interface observed in other samples,[7] due to anodization, is not detected in this case. These profiles are presented in Section 3.

Section 1
INTERFACE STRUCTURE

In this study we have characterized the electronic structure of HgCdTe interfaces with two types of passivation: anodically grown oxide, and photochemically deposited SiO_2 (Photox). The more optimum interface was produced with photo SiO_2. These interfaces were characterized using capacitance-voltage C-V techniques as well as DLTS.

The capacitance technique is very interface sensitive and allows us to determine directly the surface state density, N_{SS}.[8] Other properties of the interface region, such as hysteresis, flatband shift, and carrier concentration profiles, are also of interest.[9] DLTS is employed to characterize traps in the interface region, since the technique is less biased toward surface states. Distortions of bulk properties due to surface treatments have been reported which extend hundreds of Angstroms below the surface.[10] These changes affect carrier concentration, trap activity, stoichiometry, and even electrical type. Properties of the passivation layer itself are not the focus of this study and are covered extensively elsewhere.[11-13]

Ellipsometry is used to monitor the HgCdTe surface condition during prepassivation processing. It is by comparison of these results with interface structure that our model of the passivated interface emerges.

1.1 SAMPLE PREPARATION

Measurements were done on MIS devices formed on zone melt and solid state recrystallized bulk material annealed n-type to 10^{14} to 10^{15} cm^{-3} at x = 0.3. The basic surface preparation used consisted of a chemical polish in 2% Br_2-DMF (dimethylformamide) followed by a light Br_2-ethylene glycol spray etch. Each step was followed by a solvent rinse to remove residue. The surfaces were passivated with either anodization or deposition of SiO_2 by the patented 'Photox'™ process. The SiO_2 is deposited to a standard thickness of 1500Å, which yields devices of about 60 pF. Metal contacts were deposited to form capacitors with an area of 2.04×10^{-3} cm^2.

1.2 RESULTS

A comparison of C-V results of the best interfaces achieved with each type of dielectric is shown in Table 1.

Table 1. Comparison of C-V Results

	Anodic Oxide	SiO_2
FLATBAND VOLTAGE (charges/area)	-2.0V (1×10^{12} cm^{-2})	-0.4V ± 0.5F ($< 1\times10^{10}$ cm^{-2})
HYSTERESIS	0.5V	< 0.2V
SURFACE STATE DENSITY N_{SS} (minimum)	1×10^{11} cm^{-2} eV^{-1}	1.4×10^{10} cm^{-2} eV^{-1}
STORAGE TIME	85 sec	1.8×10^{3} sec
SURFACE RECOMBINATION VELOCITY	1.6×10^{2} cm sec^{-1}	1×10^{-2} cm sec^{-1}

The density of interface states (N_{SS}) as derived from the difference of measured and theoretical quasistatic capacitance, is shown in Figure 1 for both types of dielectrics. An additional anodic oxide curve is shown for comparison which is derived from the difference between quasistatic and high frequency (1 MHz) capacitance. There is good agreement of the two techniques between accumulation and midgap regions which is the range of validity of the second technique. We take the difference of these curves as a measure of the uncertainty of N_{SS}.

Both interfaces produce qualitatively similar types of N_{SS} curves. They are free of discrete states and span the entire gap region. The general curvature is also the same in both cases. Major differences in curvature can arise from a difference in bonding at the interface.[14] We see no evidence of any such difference for these interfaces. The principal difference is the lower midgap minimum seen in SiO_2, in some cases by an order of magnitude. As shown in Table 1, SiO_2 interfaces exhibit a quantitatively better structure than anodic oxides. The most striking difference is the large flatband shift for anodic oxides. This arises from a fixed positive charge in the passivation layer itself on the order of 1×10^{12} cm^{-2}. There is evidence this can be controlled by the anodization process.[15]

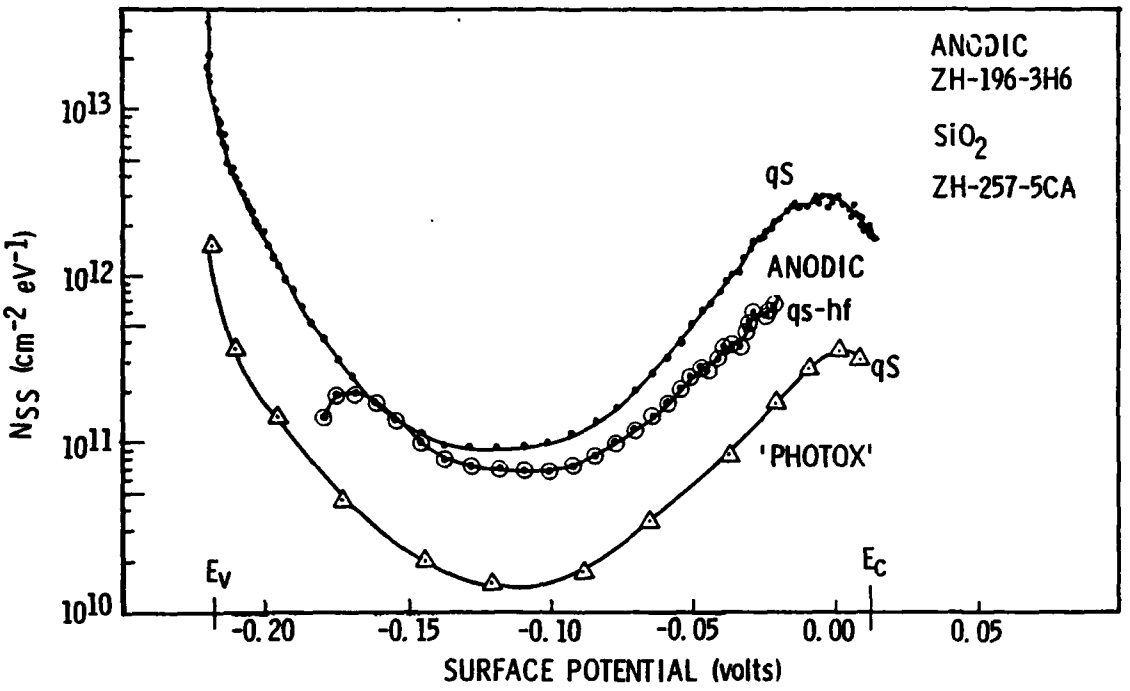

Figure 1. Density of Interface States (N_{SS}) for SiO_2 and Anodix Oxide on $Hg_{0.7}Cd_{0.3}Te$.

The surface of all the wafers used were prepared using the above process, with ellipsometry used to monitor the surface condition during processing. Ellipsometry is a technique where circularly polarized light is reflected from the surface of a sample. Measurement of relative change in amplitude and phase of the parallel and perpendicular components give an indication of thickness and refractive index of thin films on the surface. The parameter Δ is seen to decrease as film thickness increases. Immediately following the chemical polish, Δ is typically in the region of 147, which is near the value for a nominally clean HgCdTe surface. After the subsequent etch and clean-up and immediately prior to application of the passivation, Δ has dropped to the range of 140 to 143 (Figure 2). This decrease of 5 degrees is consistent with the growth of a thin film on the order of 15 to 20Å thick for very thin films. The dependence of Δ on thickness is not significantly affected by the refractive index, as illustrated in Figure 3. Thus ellipsometry gives very little information on the composition of the thin film seen. Wafers processed in this manner have also been examined by Auger electron spectroscopy, however, and indicate that, the film is a thin layer of Te oxide.[16] Comparison of sputter/Auger data of anodic oxides subsequently grown on these wafers indicates the oxide layer formed during processing is compositionally different.[17]

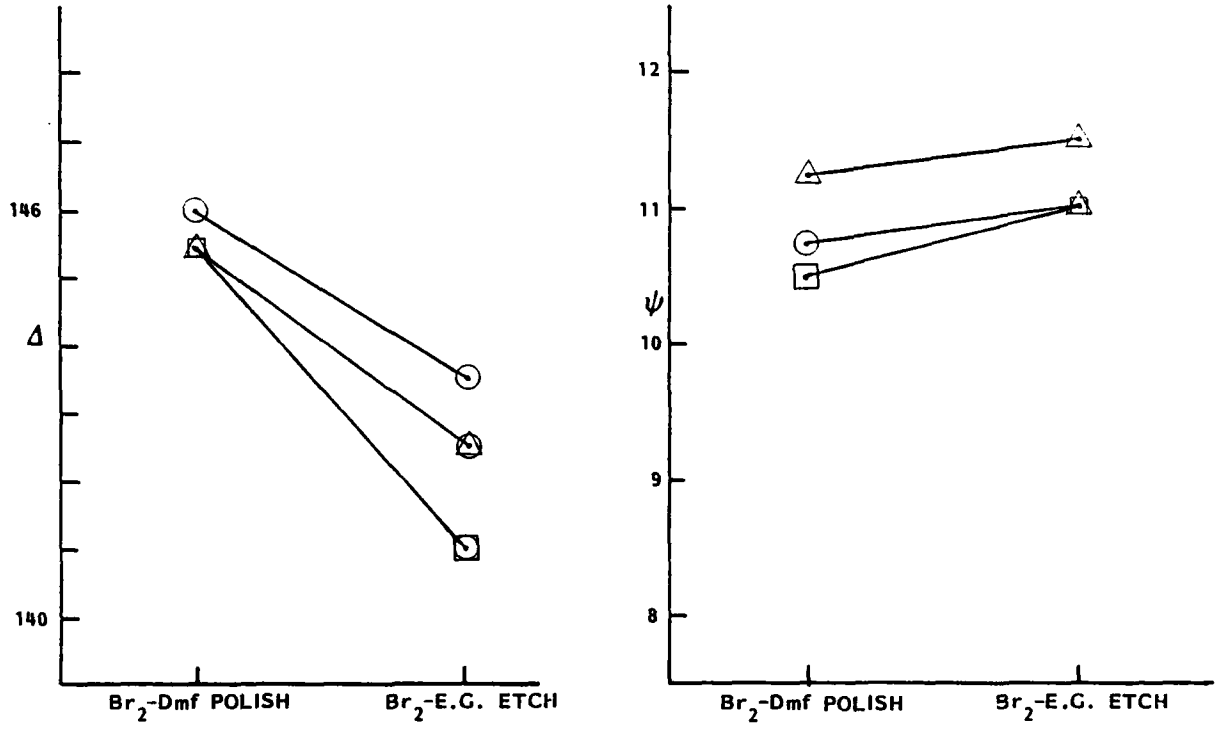

Figure 2. Effect of Surface Treatments on Ellipsometer Parameters

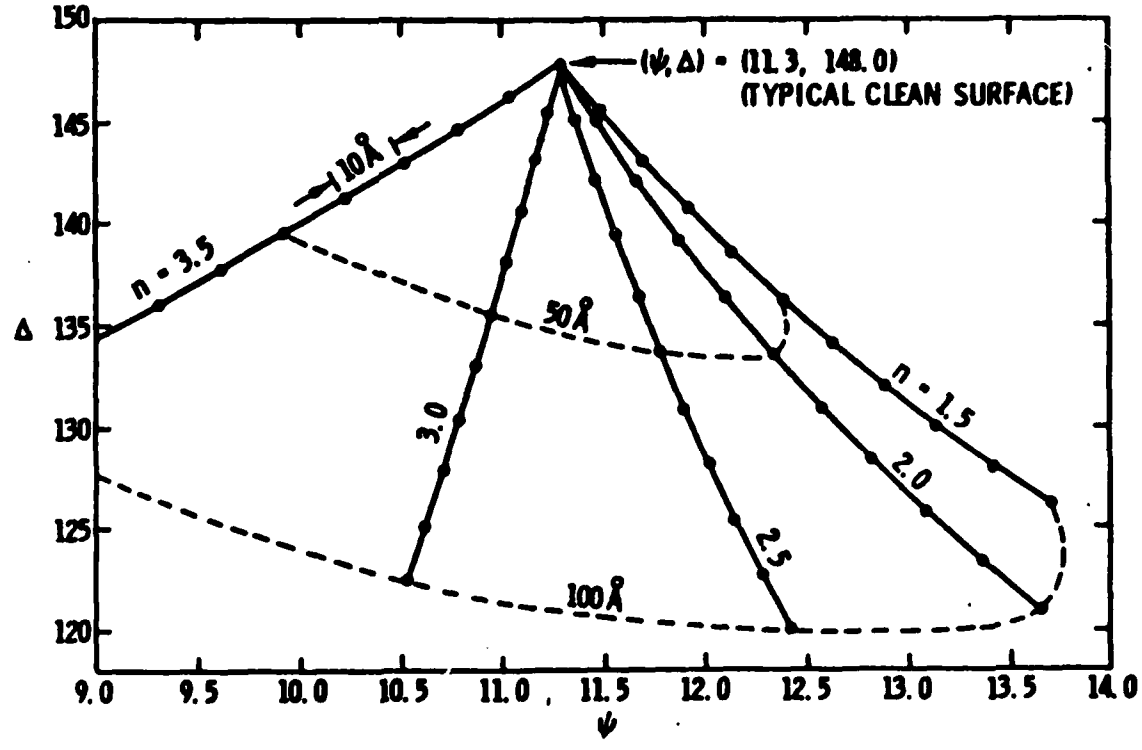

Figure 3. Calculated Values of Δ and Ψ for Thin Films on HgCdTe

The anodic oxide is a complex oxide consisting of Te, Cd, and a small percentage of Hg, while the process induced layer is principally Te-oxide. It is on this more simply oxidized surface that the better interfaces are made.

We have found that a higher Δ value can be recovered by a variety of techniques immediately before passivation. These steps have a strong effect on the structure of the resulting interface. A long dip etch in Br_2 DMF recovers a Δ of 147 and gives capacitance curves as shown in Figure 4 when SiO_2 is applied. As expected, flatband voltage is unaltered. However, the hysteresis has increased from 0.2V to 0.8V. Also, the slope of the curve through the flatband region is lower, indicating an increase in surface state density. In addition, then, to giving a lower surface state density, it appears that the existence of the oxide layer at the interface inhibits the diffusion of carriers into states in the SiO_2 and lowers the hysteresis.

A second technique was to treat the wafer with HF followed by a Br_2 ethylene glycol spray etch. This produced a high Δ surface but with a much poorer N_{SS} curve. As shown in Figure 5, the midgap minimum had increased to

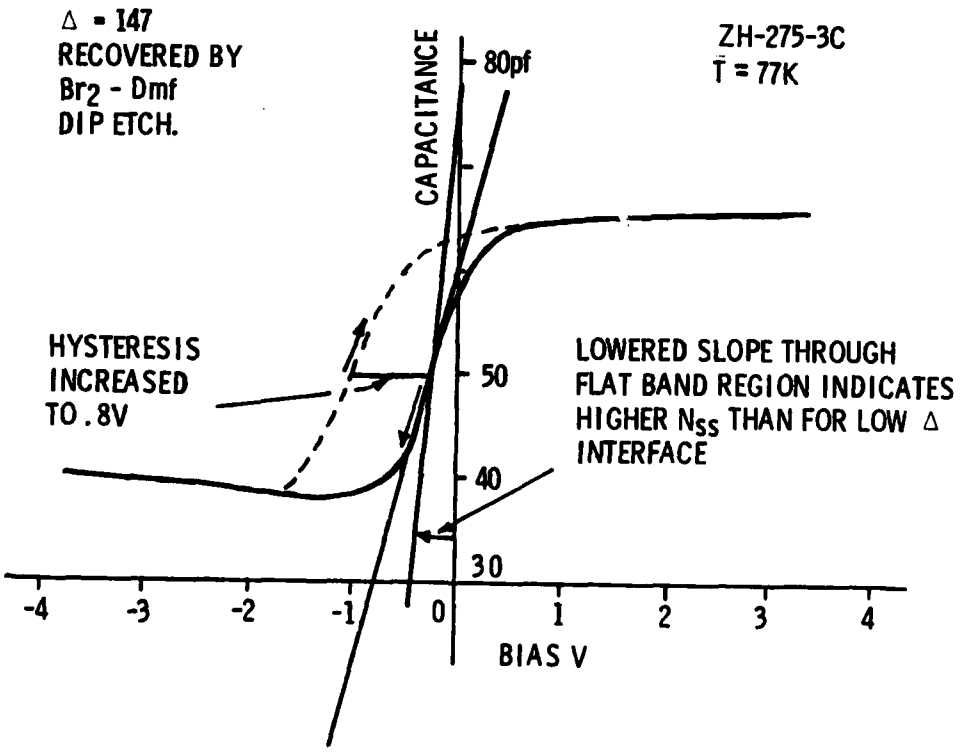

Figure 4. High Frequency (1 MHz) C-V Curve of SiO_2 Layer on Clean (Δ = 147) Substrate. Hysteresis is Increased to 0.08V and Slope Through Flatband is Lowered.

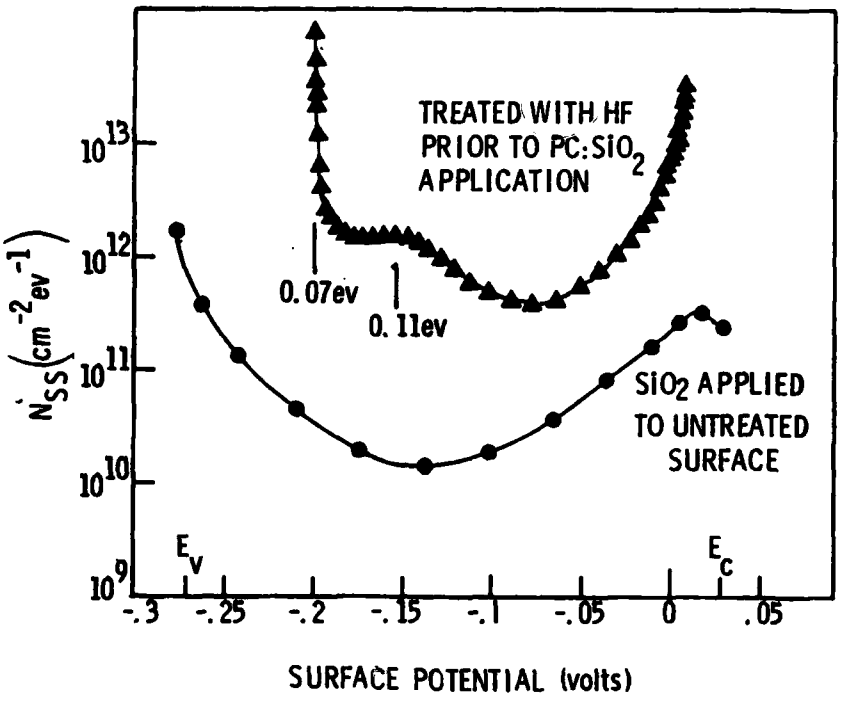

Figure 5. Density of Interface States (N_{SS}) For SiO_2 on a Surface Treated with HF Compared to an Untreated Surface.

5×10^{11} cm^{-2} eV^{-1}, with evidence of discrete states at 0.1 eV and 0.07 eV above the valence band maximum. The latter has a high enough concentration to pin E_f. In addition to removing the oxide layer, defects have been produced which strongly alter the bonding with deposited SiO_2. These defects are induced deep enough that several micrometers of HgCdTe had to be polished away before an undamaged interface could be produced.

In a separate set of measurements on devices similar to those of Table 1, the region below the interface was examined using DLTS. The data are shown in Figure 6. The spectra of both types of interfaces are similar in their major structure in that they are dominated by the same large peak corresponding to an electron trap. The large peak is seen to be asymmetrically broadened indicating a possible field dependence to the activation energy. An Arrhenius plot of the of the DLTS data gives $E_T = E_C - 0.02$ eV. Correction for a field effect yields an energy of $\sim E_C - 0.07$ eV or about 1/3 the gap energy in this material. Bulk trap levels at 1/2 E_g and E_C - 1/4 E_g have been previously reported.[18]

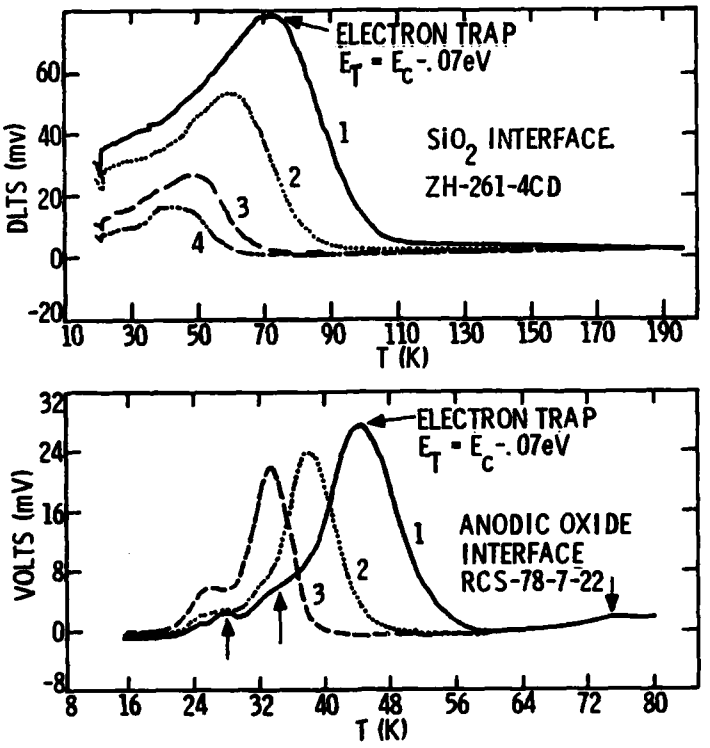

Figure 6. Comparison of DLTS Spectra for Anodic Oxide and SiO_2 Interfaces. Both Spectra are Dominated by an Electron Trap with $E_A \approx 1/3\ E_g$ (0.07 eV).

Depth profile data taken of the SiO_2 interface are shown in Figure 7. These are obtained by maintaining a fixed rate window while the pulse height is varied between two successive DLTS cycles. This is a standard technique for profiling traps in the depletion region of a diode. In our MIS devices we have the added effect of producing different band bending on each pulse so that we are at the same time profiling in energy across E_g and in depth through the depletion region. From our capacitance measurements we can convert bias pulse height to surface potential. This is shown in Figure 8. From this data we see that the curves shown in Figure 7 are consistent with two types of distributions: a distribution of interface states near the valence band, or a bulk trap level near the conduction band which is depleted near the interface. These alternatives are illustrated schematically in Figure 9. As the interpretation of interface states giving rise to this signal is inconsistent with the activation energy and does not comply with N_{SS} derived from C-V data, we conclude that we are seeing the effects of bulk traps.

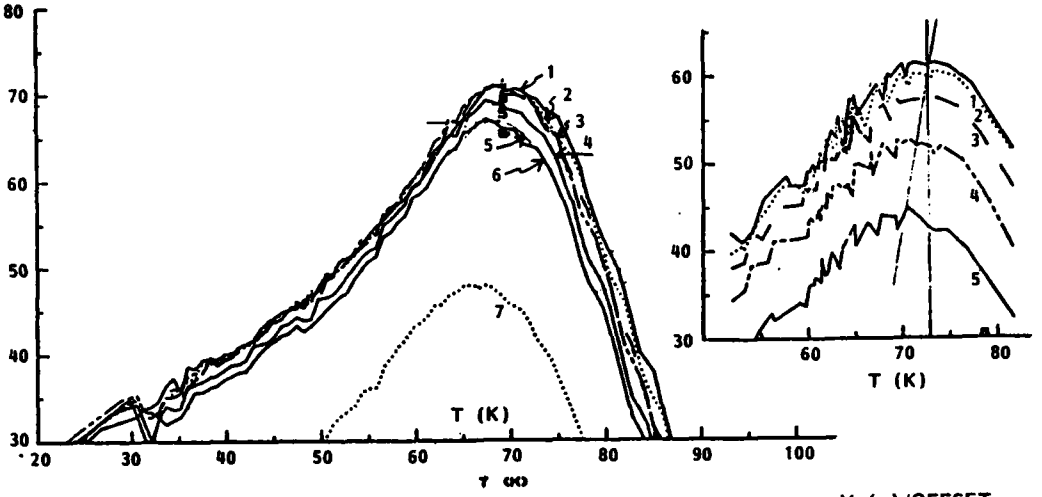

CURVE #	t_1 (ms)	t_1^* (ms)	t_w (μs)	V_p(v)/OFFSET
1	0.50	1.00	900.00	4.99 / -4.99
2	0.50	1.00	900.00	3.00 / -4.99
3	0.50	1.00	900.00	1.00 / -4.99
4	0.50	1.00	900.00	0.00 / -4.99
5	0.50	1.00	900.00	-2.50 / -4.99
6	0.50	1.00	900.00	-3.50 / -4.99
7	0.50	1.00	900.00	-4.50 / -4.99

V_p(v)/OFFSET
-3.50 / -4.99
-3.75 / -4.99
-4.00 / -4.99
-4.25 / -4.99
-4.50 / -4.99

Figure 7. DLTS Spectra Taken of SiO_2 Interface. The Rate Window is Held Constant While Pulse Height is Varied to Provide Depth Profile Information.

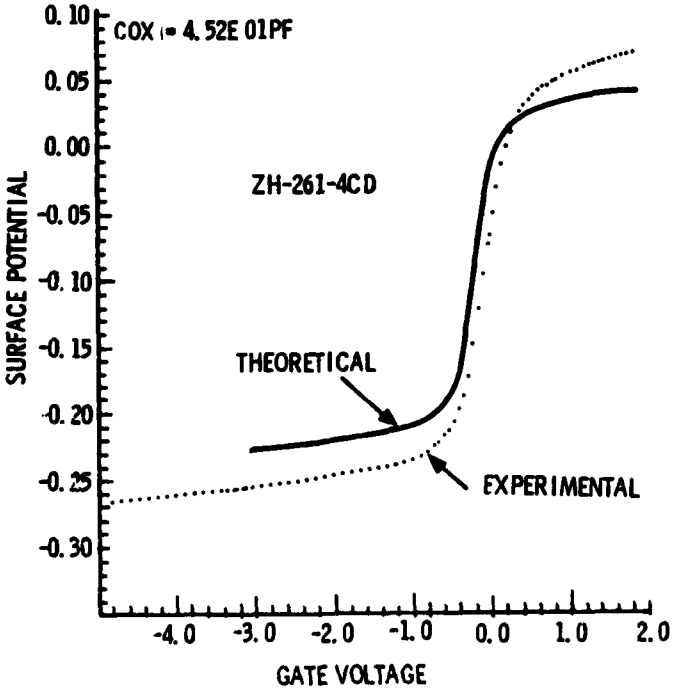

Figure 8. Surface Potential Versus Gate Bias Derived from C-V.

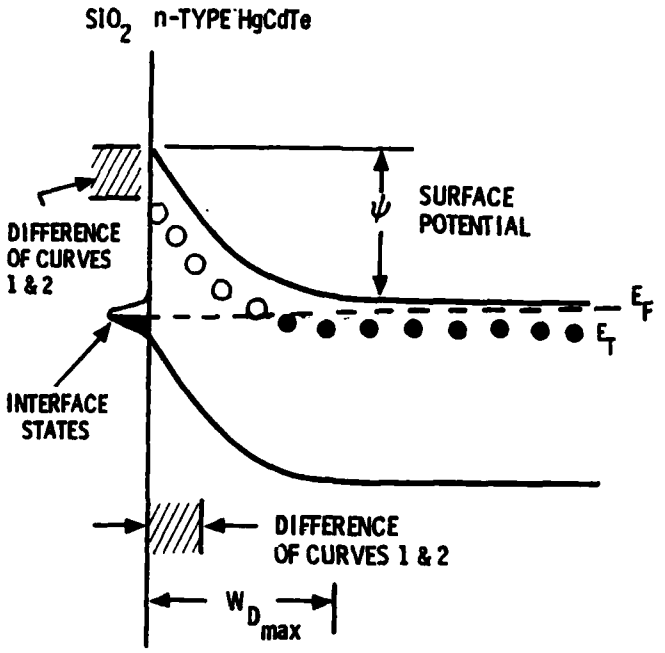

Figure 9. Schematic Representation of Possible Interface Structure seen by DLTS.

Based on this interpretation, a relative concentration is derived and plotted in Figure 10. This shows a relative depletion of this trap level as the interface is approached. Whether this is due to an alteration of the activity of a certain center or an actual population change will be the subject of further studies.

While action on HgCdTe such as that involved in chemical polishing, has been seen to cause substantial Hg to be depleted in the surface region, electroreflectance measurements have now monitored these effects up to 100Å deep.[19] Hg depletion has also been detected by Morgen, et.al., using sputter/Auger on both anodic interfaces and on wafers prepared for anodization with the altered stoichiometry is attributed solely to the preanodization processing.[20] As these wafers were prepared in the same way as the SiO_2 interfaces studied by DLTS, it is likely we are detecting the same alteration on a deeper scale. This is due to the higher sensitivity of probing the electronic properties of a trap rather than measuring compositional changes.

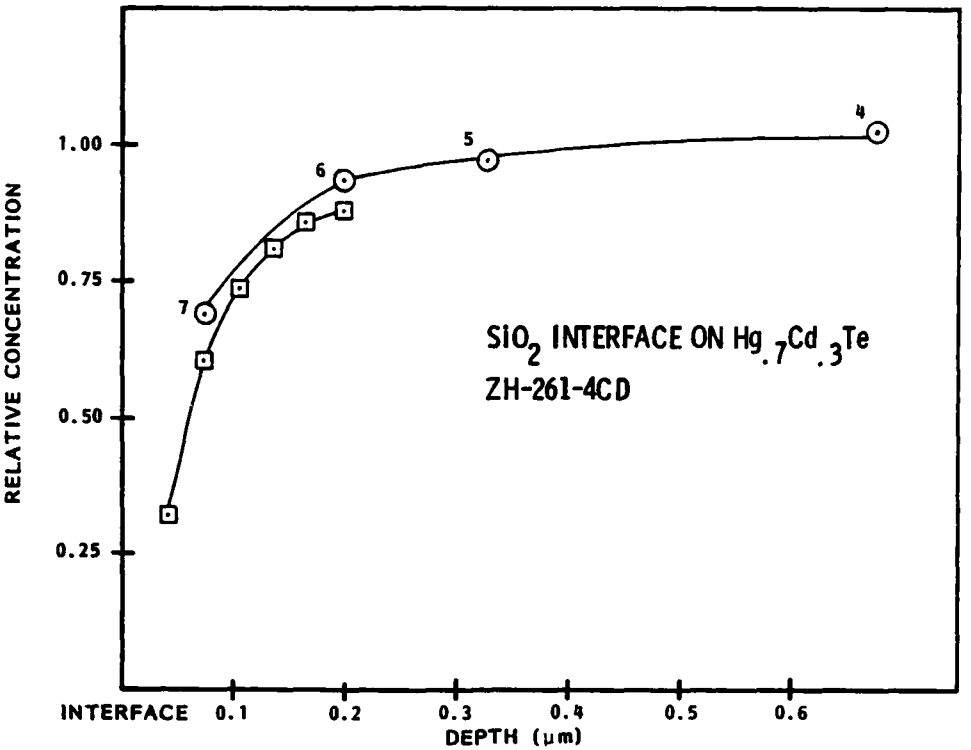

Figure 10. Relative Depth Profile of the Bulk Trap Derived from DLTS Data of Figure 7.

1.3 CONCLUSION

The highest quality passivated interface seen to date has been produced with Photox™ SiO_2. These interfaces show no discrete surface states, an N_{SS} minimum of 1.4×10^{10} cm^{-2} eV^{-1}, essentially no flatband shift and hysteresis values as low as 0.2 eV. The electronic structure of this interface is most likely due to an oxide interlayer formed during predeposition processing. That oxide is not of the same composition as formed by anodization but a thin layer of tellurium oxide. The actual oxide formed depends on the surface stoichiometry and defect density, both of which are dictated by details of the surface treatments used before passivtion. These surface treatments have also been seen to affect electronic activity to 1000Å from the interface.

Section 2

UPS STUDY OF THE INTERACTION OF HgCdTe WITH ACTIVATED OXYGEN

2.1 INTRODUCTION

Earlier studies of the interaction of oxygen with clean HgCdTe surfaces demonstrated this material to be highly inert to dry molecular oxygen in the ground state, (i.e., unexcited) and that oxidation proceeded if activated oxygen was used.[21-23] In the case of oxygen activated by an operating ionization guage,[24] exposure to 3.6×10^6 L (1 Langmuir = 10^{-6} torr-sec) resulted in a loss of Hg from the cleaved (110) surface without oxygen uptake; for a subsequent exposure roughly 100 times greater, further Hg depletion was observed together with evidence of oxidized tellurium. Thus it appeared oxidation occurred via a two step process in which Hg loss preceded oxide formation.

To investigate this process in more detail, a systematic series of exposures to oxygen in the presence of the operating ionization guage were performed on cleaved (110) surfaces of CdTe, HgTe, and $Hg_{0.78}Cd_{0.22}Te$. The oxygen uptake was monitored by UPS and XPS as in the previous case. For the alloy sample, exposures were performed in two ways: with the sample positioned so that there was no direct path between the sample surface and excitation source (ion guage) and with the sample placed in direct line of sight with the guage. Oxygen uptake for the out of line-of-sight geometry did not occur, as evidenced by the lack of O 2p emission in valence band spectra. This suggests that atomic or ionic oxygen may be necessary for strong oxidation rather than the meta-stable O_2-singly excited state of the molecule (which is important for III-V oxidation). A depletion of surface Hg is indicated by the XPS results, however, due to the "out of line-of-sight excited oxygen." Subsequent exposure of this surface at the line-of-sight position resulted in oxide formation characterized by a chemical shift in the Te 3d core level emission. While the evidence for a two step process is different from the earlier experiments,[25] the data obtained are consistent with this model in as much as oxide formation occurred on a surface which was deficient in Hg following the indirect exposure. In addition, the experiments yield information on the different roles of Hg and Cd in oxide formation for the alloy; data of this kind are supplemented by monitoring oxygen uptake of cleaved samples of HgTe and CdTe as well.

The difference in experimental conditions is important to consider when comparing the present results to those obtained previously.[26] Factors such as geometry and oxygen pressure can have an influence on the nature and amount of excited species arriving at the surface. These variables will be the subject of further study. A description of the experimental procedure used for the current study is given and a discussion of the results obtained follows.

2.2 EXPERIMENTAL

A description of the experimental apparatus used as well as an outline of the exposure procedure have been given elsewhere[27]; details of the exposure used including relevant changes in equipment are discussed. For this study, clean surfaces of CdTe (II-VI, Inc.), HgTe (SBRC), and HgCdTe ($x = 0.22$, SBRC) were prepared by cleaving along a (110) plane in vacuum ($p < 10^{-10}$ torr).

In the case of CdTe, the oxygen doses were carried out in the main experimental chamber in a manner similar to that in reference 12. The pressure and duration of each increment used to achieve a given accumulated dose are shown in Table 2. Oxygen pressure was monitored by a cold cathode gauge for all but the highest exposure, for which a millitor gauge (Varian Assoc.) was used. A Bayard-Alpert ionization gauge operating at 0.4 mA emission current and located out of direct line-of-sight from the sample surface served as an excitation source for the oxygen. For pressures of 10^{-3} torr and above, the gas was removed at the end of the exposure period by an auxiliary pumping station[28] prior to valving on the main ion pump.

For the HgTe and alloy samples, gas exposures were performed in an evacuated appendage separated from the main chamber by an all-metal straight through valve. This appendage consists of a linear motion feedthrough operating through the valve for transferring the sample from the main chamber, a leak valve and oxygen bottle, and an ionization gauge for both exciting the oxygen and measuring the pressure. The gauge and oxygen source were used in two configurations. In one, they were located in the arm of a cross perpendicular to the linear motion and behind the sample surface. In the second location, the sample surface, gauge, and gas inlet were colinear with the sample placed at one position by linear motion, but not in a direct line with the sample placed at another. The auxiliary pumping station, connected through an all-metal valve to this volume, was used to pump the oxygen following an exposure, and pumping at a low rate was maintained during the exposure to minimize carbon contamination of the sample.

Table 2. Pressure (torr), Time (sec), and Ionization Guage Emission Current (mA) used for the Exposure Increment need to Reach a Given Accumulated Exposure (Langmuir).

ACCUMULATED EXPOSURE (L)	CdTe	HgTe	HgCdTe, x = 0.22		
			OUT OF LINE-OF-SIGHT CONFIGURATION 1	OUT OF LINE-OF-SIGHT CONFIGURATION 2	DIRECT LINE-OF-SIGHT
10^4	10^{-5}, 1000, 0.4	10^{-4}, 100, 0.4	10^{-5}, 1000, 0.4	10^{-5}, 1000, 0.4	10^{-4}, 100, 0.4
2×10^4		10^{-4}, 100, 0.4			10^{-4}, 100, 0.4
5×10^4		3×10^{-4}, 100, 0.4	4×10^{-5}, 1000, 0.4	4×10^{-5}, 1000, 0.4	3×10^{-4}, 100, 0.4
10^5	10^{-4}, 900, 0.4	5×10^{-4}, 100, 0.4	5×10^{-5}, 1000, 0.4	2.5×10^{-4}, 200, 0.4	5×10^{-4}, 100, 0.4
2×10^5		10^{-3}, 100, 0.4			10^{-3}, 100, 0.4
5×10^5			4×10^{-4}, 1000, 0.4	2×10^{-3}, 200, 0.4	3×10^{-3}, 100, 0.4
10^6	10^{-3}, 900, 0.4	8×10^{-3}, 100, 0.4	5×10^{-4}, 1000, 0.4	2.5×10^{-3}, 200, 0.4	5×10^{-3}, 100, 0.4
2×10^6					
5×10^6		4.5×10^{-2}, 100, 0.1	4×10^{-3}, 1000, 0.4	3.8×10^{-6}, 100, 0.2	3.2×10^{-2}, 100, 0.2
10^7	10^{-2}, 900, 0.4			2.7×10^{-2}, 200, 0.2	
3×10^7		2.2×10^{-1}, 100, 0.04			

By performing the exposure sequences in the appended volume, pumping time following a dose was reduced and the main chamber pressure preserved.

Pressures and duration of exposure are given together with the ionization gauge emission current in Table 2 for the accrued exposures for HgCdTe and HgTe. The pressure was monitored with the ionization guage in the range up to 10^{-2} torr; a DV-6 thermocouple gauge remotely situated at the auxiliary pump cart was used at higher pressured.

Exposures out of line-of-sight of the gauge were performed on fresh cleaves of the alloy using the gauge in both configurations. Because oxygen uptake was not evident in the UPS data for a dose of 10^7 L in either case, the surface exposed in the second configuration was then used in the direct line-of-sight exposure sequence. The procedure involved adjusting the oxygen pressure and gauge emission current to the required values with the sample in the out of line-of-sight position, then sliding the sample with the linear motion to the line-of-sight location for the duration of the exposure, returning the sample to the original position, and removing the oxygen. In this way, the duration of the exposure could be reduced while negligible inaccuracy was added to determination of the exposure. The total time required to transfer the sample from the main chamber, dose it, and replace it was roughly 40 minutes.

A differentially pumped He discharge lamp with monochromator provided 21.2 eV radiation for the UPS measurements while a Mg (1253.6 eV) or Al (1486.6 eV) anode was the excitation source for XPS measurements for CdTe or the samples containing Hg, respectively. Emitted electrons were energy analyzed using a double pass cylindrical mirror analyzer resolution with axis normal to the sample surface. The analyzer resolution was 0.18 eV for UPS and 0.5 eV in the XPS measurements.

2.3 RESULTS AND DISCUSSION

2.3.1 CdTe

The UPS spectra for clean and oxygen exposed CdTe are given in Figure 11. The number of electrons is plotted versus the electron initial state energy. The origin of the energy scale is the valence band maximum (VBM) for each curve. The spectra are presented as recorded, without normalization.

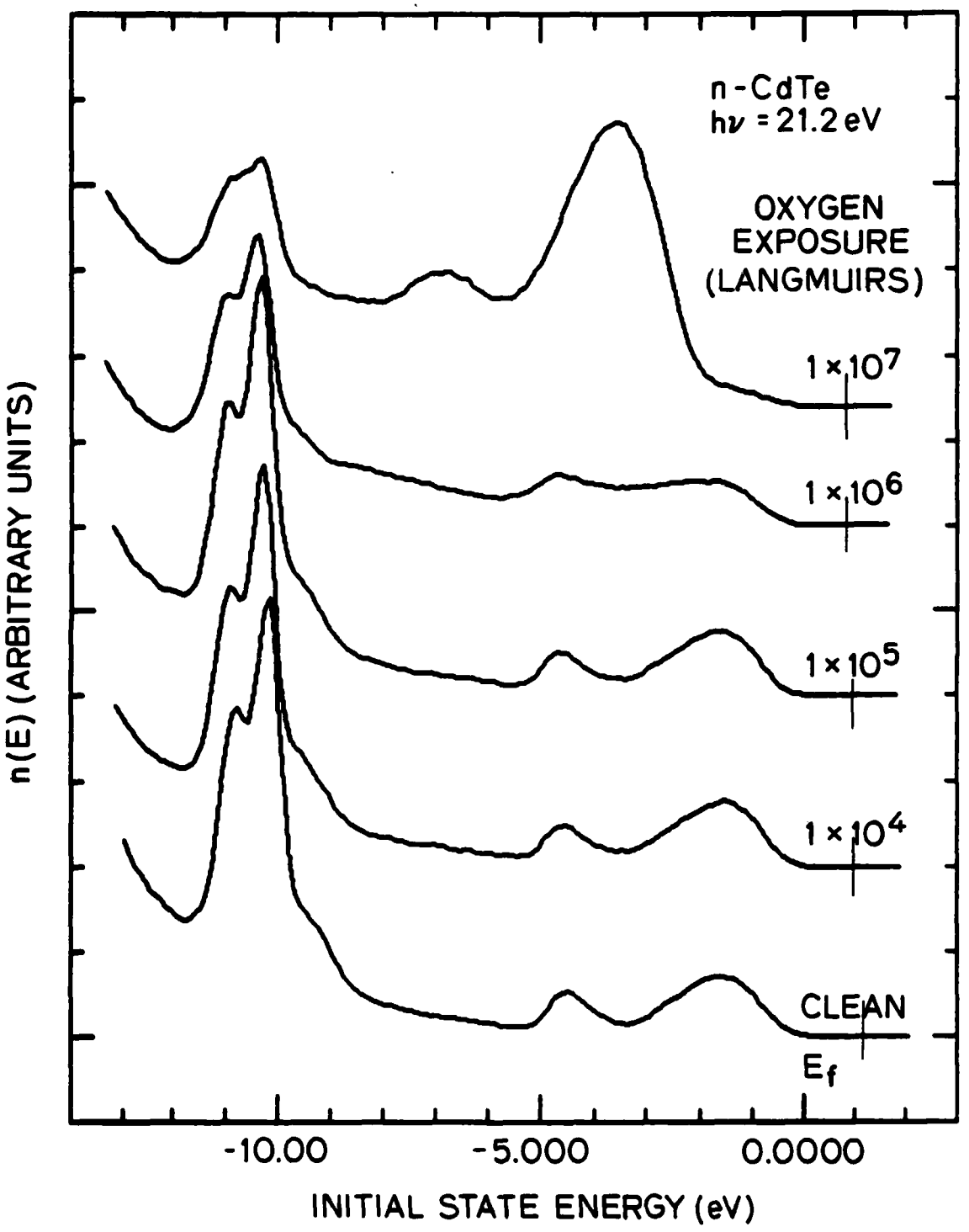

Figure 11. Photoemission Spectra (21.2 eV) of CdTe Showing the Effect of Oxygen Exposure on Valence Band Structure and the Cd 4d Core Lines.

In the clean surface spectrum, valence band emission extends to around -5 eV, and the spin orbit split Cd 4d levels appear near -10.4 eV. The Fermi level position for the cleaved surface lies 1.1 ± 0.2 eV above the VBM as indicated in the figure. Because the sample was n-type (In doped) with a carrier concentration greater than 10^{17} cm^{-3}, the bulk Fermi level position is expected to be near the conduction band minimum; hence, the cleaved surface E_f is pinned by ~ 0.4 eV.

For an exposure of 10^4 L, the Fermi level shifts 0.2 eV closer to the VBM. The Cd 4d levels appear to shift to higher binding energy by 0.1 eV. From the XPS data, no chemical shift is observed for the Te 3d or Cd 3d core lines, although both levels are attenuated in strength relative to the clean surface. While oxygen 1's emission is weak in the XPS spectra, carbon intensity corresponding to 0.1 monolayer is observed.

The changes observed following the 10^4 L exposure continue for doses totaling 10^5 and 10^6 L (Figure 11). Oxygen-induced emission near -3.5 eV increases in strength with added exposure. In the 10^6 L curve, a weak, broad feature appears near -8 eV. From the XPS data, the carbon to oxygen ratio is roughly unity following this exposure. The Te and Cd core level intensity continues to decrease suggesting the build-up of an adsorbed layer on top of the surface. For up to 10^6 L, the chemically shifted Te line is not observed.

Rapid oxygen uptake occurs for the highest exposure, resulting in prominent structure at -3.5 and -6.9 eV. This second peak may have its origin in the broad feature near -8 eV in the 10^6 L curve, a point which will be examined in future study. (A reduction in valence band width of this type occurs for metallic Cd.[29]) The Cd 4d spin orbit splitting is no longer resolved, indicating disordering of the surface, and the 4d levels are further reduced in intensity. In the XPS data, a chemically shifted component of the Te 3d core lines appears at 3.5 eV higher binding energy indicating Te-oxide formation. The unshifted (bulk) Te emission is further reduced as is the Cd 3d intensity; the attenuation of the Cd emission is less than that of the Te, however, suggesting incorporation of Cd in the oxide layer. For the highest exposure, the Fermi level at the surface has shifted by 0.35 eV from the cleaved surface position to approximately 0.75 eV from the VBM.

For the purposes of analysis, one can use a layered model to examine the variation in core line intensity in the XPS spectra. Such a model for the oxide-substrate system supposes an abrupt planar interface between an homogeneous oxide layer and an homogeneous (bulk) semiconductor.

Within the context of such a construct, the relative intensity of the bulk and chemically shifted (oxidized) Te 3d core level emission indicates an oxide layer thickness of ~ 9 Å; where the additional assumption of constant density for the Te atoms in both the bulk and oxide has been used. The ratio of oxygen to oxidized Te is 2.4, while the ratio of Cd in the oxidized layer to oxidized Te is 1.45. (The ratio of Cd to Te in the bulk in 1.0.)

The model discussed serves only to aid in analysis and is not taken to describe the actual oxide-substrate system. The Cd enrichment of the oxide layer relative to the bulk calculated in this way indicates the distribution of Cd likely differs from homogeneous; a higher concentration of Cd near the surface, for example, would explain the apparent enrichment. In a study of CdTe oxidation using electron beam probes, the oxide was determined to be TeO_2[30]; the Cd component observed in the present case could possibly desorb under electron irradiation, particularly if it is a surface species. This possibility can be tested in future work, and information obtained on the stages of oxidation for exposures between 10^6 L and 10^7 L and at saturation, if such a point is reached.

2.3.2 HgTe

Energy distribution curves (EDS) obtained using HeI (21.2 eV) radiation for clean and oxygen exposed HgTe are presented in Figure 12. As was the case in Figure 11, the EDC are plotted against initial state energy relative to the VBM. Since HgTe is a semimetal, this is also the location of the Fermi level which is therefore not shown. These curves have been normalized to the height of the distribution at -11 eV.

As the oxygen exposure increases, oxygen structure in the valence band (near -4.4 eV) steadily increases while the emission from the spin-orbit split Hg 5d core levels at -8.1 and -10.0 eV steadily decreases as does valence band emission near -1.0 eV. The intensity between the valence bands and Hg 5d 5/2 peak also increase with oxygen exposure; this could be due either to scattered electrons from the rising O 2p peak (-4.4 eV) or an oxygen feature similar to the peak at -6.9 eV for CdTe. for exposures in excess of 2×10^5 L, the oxygen uptake appears to saturate; little difference in oxygen or Hg 5d emission is apparent in the UPS spectrum for these doses (Figure 12). Because the exposures to total 5×10^6 and 3×10^7 L were preformed with reduced emission

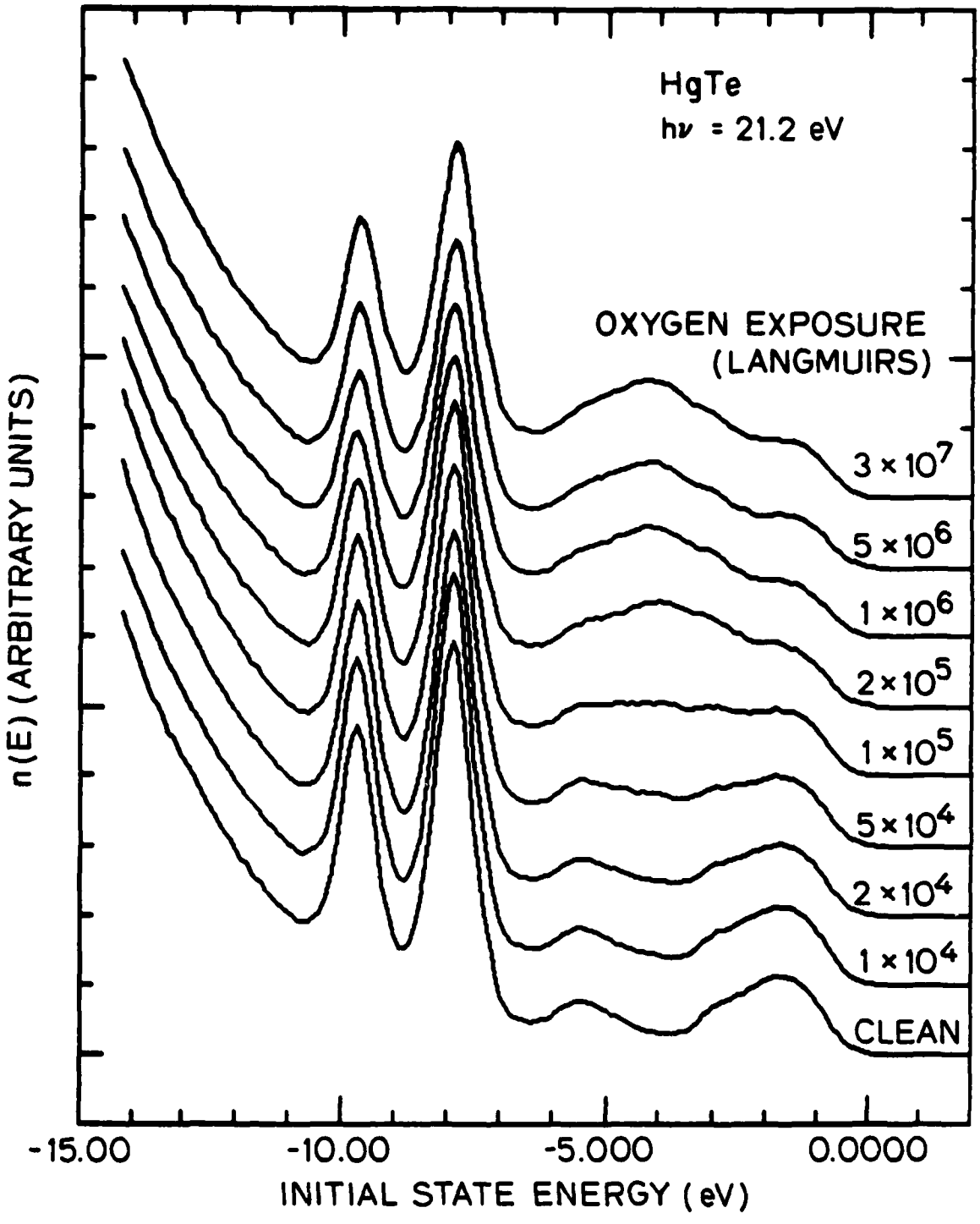

Figure 12. Photoemission Spectra (21.2 eV) of HgTe Showing the Effect of Line of Sight Oxygen Exposure on Valence Band Structure and the Hg 5d Core Line.

in the ionization gauge, the dose of activated oxygen may not increase as fast as the total exposure. This suggests a reduced rate of uptake rather than saturation as observed, however, and would not apply to the 10^6 L exposure.

The XPS data are available only up to 2×10^5 L due to equipment failure. A shifted Te 3d peak appears at 3.7 eV higher binding energy following the 5×10^4 L exposure and gains in strength with increasing coverage. A model calculation such as described for CdTe yields an oxide layer thickness after the 2×10^5 L dose of 2 Å. Based on the UPS data, the overlayer does not appreciably grow at higher doses so that this value is approximately the saturation coverage. The ratio of oxygen to oxidized Te increases from 1 at 5×10^4 L to 1.8 at 10^5 L.

The behavior of HgTe is thus quite different from that of CdTe. In the case of CdTe, no evidence of saturation was obtained for exposures up to 10^7 L, while the uptake on HgTe slows markedly around 2×10^5 L for the geometry used. In addition, the cation (Cd or Hg) is observed as a part of or on the surface of the oxide for CdTe but not HgTe. Finally, the binding energy of the O 2p peak in the UPS data is greater in the case of HgTe.

2.3.3 HgCdTe, x = 0.22

The UPS spectra for the alloy sample are given in Figure 13 showing the effect of oxygen exposure. The reference curve is taken from the surface following exposure to 10^7 L with the sample out of direct line-of-sight but in the configuration in which the gauge and gas inlet are mounted on the appended chamber in front of the sample (see Section 2). The spectra has been normalized to the same height, -11.6 eV. The Fermi level for the clean surface occurred at 0.2 ± 0.2 eV above the VBM; the calculated bulk value is 0.1 eV at room temperature.

Oxygen uptake was not evident in the valence band spectra recorded following exposure with the sample masked form the gauge in either configuration. In the first arrangement, in which the excited species is required to make up to 4 direction changes of nearly 90 degrees to reach the sample, the Hg/Te and Cd/Te core line intensity ratios remain at the clean surface value for exposures totaling 5×10^6 L. (The variation from the clean surface value observed is within experimental error: 4% and 7% for Hg/Te and Cd/Te, respectively.) At 10^6 L, the Hg/Te ratio drops to 0.87 of the original value.

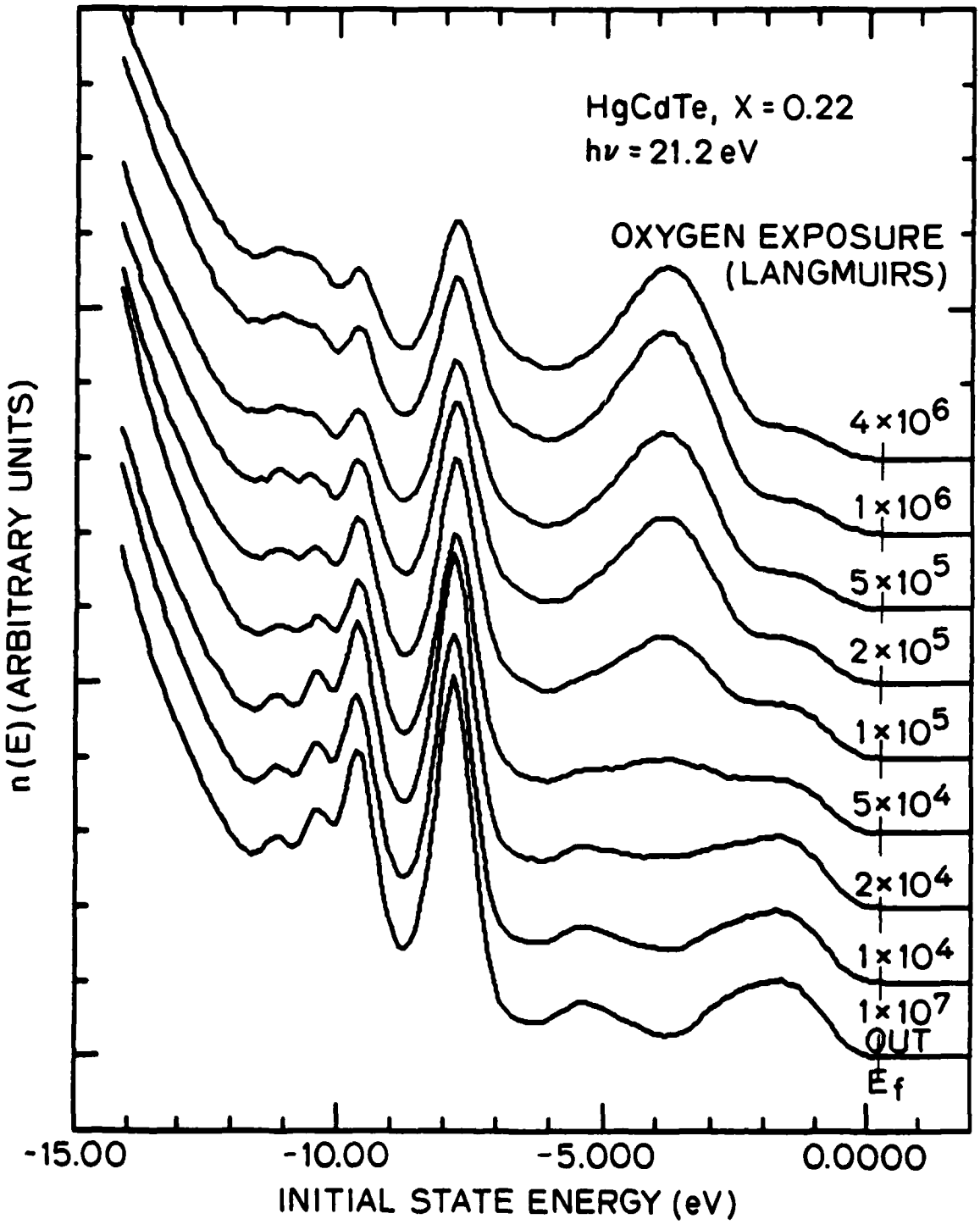

Figure 13. Photoemission Spectra (21.2 eV) from $Hg_{0.78}Cd_{0.22}Te$ Showing the Effect of Line of Sight Oxygen Exposure on Valence Band Structure and Cd 4d and Hg 5d Core Lines.

In the second configuration, arranged to reduce the scattering required for the excited species to two path changes of less than 90 degrees, the Hg/Te and Cd/Te ratios fall to a total of 9% and 4%, respectively, with the Hg/Cd ratio consistently less than the clean surface value. Because the changes involved are small, interpretation of these results to the effect of out of line-of-sight exposure or influence of geometry is tentative. These considerations are of importance, however, because the surfce used for the direct line-of-sight exposure was that exposed to 10^7 L in the second configuration. This surface apparently has Hg/Te and Cd/Te ratios reduced from that of the cleaved surface without apparent oxygen uptake.

In the UPS data for the line-of-sight sequence (Figure 13) oxygen 2p emission can be seen to grow in intensity with exposure, producing a peak after 4×10^6 L at -3.9 eV, a value intermediate to the energy of this feature for CdTe and HgTe. For the highest exposure, the Hg 5d 5/2 peak (-7.9 eV) appears somewhat asymmetric indicating a second oxygen induced peak such as was found for CdTe. As the dose increased, the concentration of Hg and Cd in the probed region changes, as evidenced by the reduction in Hg 5d core level emission relative to the lower lying Cd 4d lines in Figure 13. While the spin-orbit splitting of the Cd 4d levels is resolved for exposures up to 2×10^5 L, the two peaks can not be distinguished at higher coverages. Above 2×10^5 L, therefore, the Cd environment has become disordered.

In the XPS spectra, the ratio of intensity of the Hg 4f lines to bulk (unshifted) Te 3d emission, corrected for escape depth differences, rises from the value for the reference surface (exposed to 10^7 L in the masked position) to the original clean surface value by the time the accrued exposure reaches 2×10^4 L. As the coverage increase beyond this point, this ratio remains constant up to 2×10^5 L, as would be expected if the Hg were retained in the semiconductor but not in the oxide. On the other hand, the Cd to bulk Te ratio rises steadily to 15% above the clean surface value with increasing exposure up to 5×10^4 L. Above 10^5 L, the Hg/bulk Te ratio is somewhat higher than the clean surface value but falls again to the original level for the largest dose. The Cd/bulk Te ratio, however, continues to rise with some fluctuation to a final value 40% above that for the clean surface.

It is again instructive to examine the core line intensity within the construct of the layer model used earlier. The final oxide thickness determined in this way is 5 Å.

The ratio of oxygen to Te in the oxide has a value near three for exposures between 2×10^4 L and 10^5 L, but begins to fall at higher exposures to near two for the final coverage. The ratio of Cd in the oxide to oxidized Te is approximately 0.3 in the final film while the bulk ratio is 0.22, indicating as before a probable surface enhancement of the Cd concentration in the oxide.

2.3.4 Concluding Remarks

Because the reference surface for the line-of-sight exposure may have had Te in excess following the masked exposure, the oxidation behavior for the alloy may still be consistent with two step process observed earlier. In addition, a change in oxidation behavior seems to occur in the present experiments near an exposure of 10^5 L; the oxygen to oxidized Te ratio begins to fall at this point and the layer thickness, which increased in proportion to the exposure up to this dose, now increases more slowly. The mechanism by which HgTe oxygen uptake becomes saturated may increasingly play a role at this point, slowing the layer growth. This possibility would be apparent in a study of the oxidation under similar conditions of alloys of varying composition.

Section 3
AES-SPUTTER PROFILE OF ANODIC AXIDES ON HgCdTe

A critical issue regarding the suitability of a passivation technique is the nature of the insulator-semiconductor interface. Using Auger electron spectroscopy in combination with inert gas ion sputtering, a profile giving the depth distribution of constituents of the semiconductor and oxide can be obtained. One question we have sought to anwser by this approach is whether the substrate is depleted of Hg in the region near the anodic oxide interface. Such depletion has been reported for andoic oxides[31] in the study combining sputtering and XPS.

The samples studied were 500 Å and 1000 Å thick anodic oxide films grown of HgCdTe substrates with x = 0.21 and 0.285 by SBRC. The films were eroded by a 1 KeV Ne+ beam and Auger data recorded by automatically determining the peak-to-peak height of the relevant transitions in a dN/dE spectrum and plotting this value for each element as a function of sputtering time. A 2 μA electron beam at 5 KeV was rastered over the analyzed area of 200 μm × 200 μm, at the center of the sputter crater.

In addition to checking for Hg depletion by sputtering well past the oxide-semiconductor interface, a bare piece of HgCdTe was sputtered under identical conditions to insure the dependability of the composition measured for the oxidized sample. This second substrate was half of the same wafer as the anodized sample and had been given an identical surface preparation with the exception of anodization.

A spectrum typical of those recorded is shown in Figure 14. The sputtering beam was applied 20 minutes into the measurement; the signals to the left of this point were obtained from the unsputtered surface. The Auger signals settle to a steady value with 10 minutes of sputtering, and the semiconductor interface is reached in approximately 45 minutes of sputtering. The transitory variations in the Te and Cd signals near the interface will be the subject of further investigation. Of interest for this study is the small concentration of Hg in the oxide and constancy of the Hg signal past the interface. The Hg level obtained from the bare substrate is the same as for the anodized sample after sputtering. Thus, Hg depletion in the substrate near the interface due to anodization is not observed.

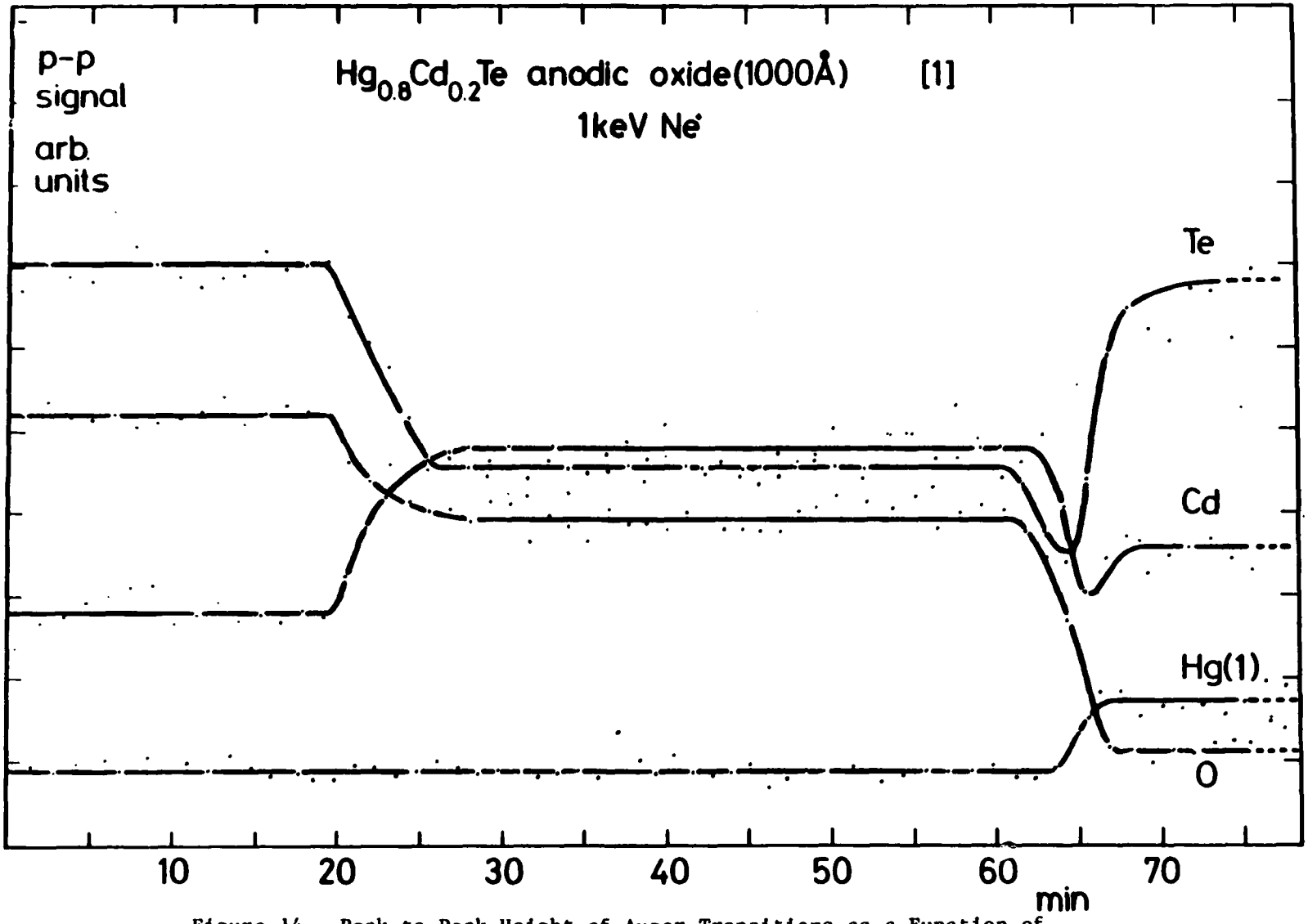

Figure 14. Peak-to-Peak Height of Auger Transitions as a Function of Time for a 1000Å Anodic Oxide on $Hg_{0.8}Cd_{0.2}Te$. Sputtering of the Oxide Film Began at the 20 Minute Mark and the Interface Occurred after About 45 Minutes of Sputtering.

Plans for final six month period

- DLTS mesurement of anodic oxide and SiO_2 interface will continue. Particular attention will be paid to the trap depth profile as well as those states which are unique to each interface.

- Very low frequency ($< 10^{-4}$ Hz) admittance spectroscopy will be done on SiO_2 MIS devices. This is expected to more sensitive to interface states than DLTS.

- Band structure calculation done in cooperation with A. Shere at SRI International will continue.

- Photoemission experiments to probe bulk and surface electronic structure will continue.

- Sputter/Auger experiments will concentrate on the SiO_2 - HgCdTe interface.

- Experiments in preparation of HgCdTe interfaces for examination by TEM will begin. This is an added task performed in cooperation with Professor R. Sinclaire at Stanford University.

- LPE HgCdTe will be produced for depth profile of composition by electroreflectance measurement in cooperation with Professor P.M. Raacah at the University of Illinois.

ACKNOWLEDGEMENTS

We gratefully acknowledge many helpful discussion with D.R. Rhiger and R.E. Kvaas, (as well as making the information displayed in Figure 3 available) also technical assistance with the DLTS experiments given by M.D. Jack, J.K. Henriksen and A. Toth of Hughes Aircraft Company and finally, to C.E. Jones and V.A. Cotton for aid in analysis of the DLTS and C-V data.

REFERENCES

[1] J.A. Silberman, P. Morgen, I. Lindau, W.E. Spicer, and J.A. Wilson, J. Vac. Sci. Technol. 21, 142 (1982).

[2] A. Lastras-Martinez, W. Lee, P.M. Raccah and V. Zender, J. Vac. Sci. Technol. 21, 157 (1982).

[3] Op cit, Reference 1, 154.

[4] Op cit, Reference 1

[5] A.-B. Chen and A. Sher, J. Vac. Sci. Technol. 21, 138 (1982).

[6] Op cit, Reference 1, 161.

[7] G. Davis, T.S. Sun, S.P. Buchner, and N.E. Byers, J. Vac. Sci. Technol. 19, 472 (1981).

[8] E.H. Nicollian and G. Goetzberger, Bell System Tech. J. 66, 1055, (1967).

[9] R. Castagne and A. Vapaille, Surf. Sci. 28, 157 (1971).

[10] Op Cit, Reference 2.

[11] J.W. Peters and D.R. Rhiger, Paper I-3, Electronics Materials Conference, 24-27 June 1980, Ithaca, N.Y.

[12] R.B. Schooler, B.K. Janousek, R.L. Ait, R.C. Carscallen, M.J. Daugherty and A.A. Fote, J. Vac. Sci. Technol. 21, 164 (1982).

[13] D.R. Rhiger, J.A. Wilson, J.M. Myrosznyk, R.E. Starr, S.L. Price, K.A. Kormos, M. Ray, J.W. Peters and H.N Rogers. Paper D-8, Meeting of the Specialty Group on Infrared Detectors 27-29 July 1982, San Diego, Ca.

[14] T. Sakurai and T. Sugano, J. Appl. Phy. 52, 1889 (1981).

[15] Op cit, Reference 11.

[16] Op cit, Reference 1, 154.

[17] Op cit, Reference 1, 161.

[18] C.E. Jones, V. Nair, and D.L. Polla, Appl. Phys. Lett. 39, 248 (1981).

[19] Op cit, Reference 2.

[20] Op cit, Reference 1, 161.

REFERENCES (continued)

[21] U. Solzbach and H.J. Richter, Surf. Sci. 97, 191 (1980).

[22] S.P. Kowalczyk and J.T. Cheung, J. Vac. Sci. Technol. 18, 944 (1981).

[23] P. Morgen, J.A. Silberman, I. Lindau, W.E. Spicer, and J.A. Wilson, J. Electron Mater. 11, 597 (1982).

[24] Ibid.

[25] Ibid.

[26] Ibid.

[27] Op cit, Reference 12.

[28] P. Pianetta, I. Lindau, C.M. Garner, and W.E. Spicer, Phys. Rev. B 18, 1782 (1978).

[29] L. Braicovich, G. Rossi, R.A. Powell, and W.E. Spicer, Phys. Rev. B 21, 3539 (1980).

[30] Atsuko Ebina, Kiyomitsu Asano, and Tadashi Takahashi, Phy Rev. B 22, 1980 (1980).

[31] Op cit, Reference 7.

APPENDIX

UNUSUAL BEHAVIOR OF $Hg_{1-x}Cd_xTe$ AND ITS EXPLANATION*

W. E. Spicer, J. A. Silberman, P. Morgen, and I. Lindau
Stanford University, Stanford, CA 94305

J. A. Wilson, Santa Barbara Research Center

An-Ban Chen, Auburn University

A. Sher, SRI International

This paper involves an unusual semiconductor alloy, $Hg_{1-x}Cd_xTe$, a breakdown of the Virtual Crystal Approximation (VCA) in that alloy (the first such breakdown in a semiconductor alloy), the success of the Coherent Potential Approximation (CPA), the "first order" explanation of these results in terms of energies of atomic valence levels, and the qualitative explanation of the unusual properties of $Hg_{1-x}Cd_xTe$ in terms of the results reported above. The genesis of the work was the use of photoemission spectroscopy. Cd and Hg core shifts are detected as a function of alloy composition and related to bonding concepts developed here.

1. INTRODUCTION

$Hg_{1-x}Cd_xTe$ is a semiconductor alloy crystallizing in the zinc blende structure in which Hg and Cd randomly occupy sites on the cation sublattice. Until recently, the electronic structure of $Hg_{1-x}Cd_xTe$ and all other semiconductor alloys has been theoretically treated within the framework of the Virtual Crystal Approximation (VCA), in which the potential used is a compositionally weighted average of the potentials of Hg and Cd. This approach has been shown to be consistent with the nearly linear variation of the bandgap in this alloy from 1.5 eV to zero with increasing Hg content [1-5] and the large electron mobility ($\sim 10^6$ cm^2/v-sec) found for narrow bandgap compositions. The volatility of Hg at slightly elevated temperature [6] and the relative ease of forming Hg vacancies, on the other hand, suggest that the bonding differs for Hg and Cd and that the electronic structure of the alloy should reflect the difference in potential of the Hg and Cd sites.

To investigate the electronic structure of $Hg_{1-x}Cd_xTe$, we have used Ultraviolet Photoemission Spectroscopy (UPS) with photon energies from 7 to 30 eV to examine single crystal alloys of three compositions and CdTe. The UPS results are compared to a recent calculation of the alloy density of states [7] computed using the Coherent Potential Approximation. CPA, unlike VCA, retains the aperiodic nature of the cation potential. In the UPS data, the upper, mainly p-like valence states within ~3.5 eV of the valence band maximum (VBM) were found to be band-like and qualitatively similar for all compositions studied in agreement with VCA calculations. In contrast, the lower lying states near 5 eV below the VBM, which are principally metal s-electron derived but contain 40% cation p-character, are more localized and reflect distinctly Hg or Cd parentage. Thus, the UPS data document differences in the contributions of the two cations to the electronic structure of the alloy and the selective breakdown of the VCA for the mainly metal s-electron band [8]. These observations are confirmed by comparison to the CPA calculation. The origin and consequences of the difference in cation bonding are discussed below.

2. EXPERIMENTAL

Clean surfaces of single crystal samples of $Hg_{1-x}Cd_xTe$ (x=0.2, 0.31, 0.39) grown by solid state crystallization (Santa Barbara Research Center) and a sample of CdTe (II-VI Inc.) were prepared by cleaving the samples along a (110) face in vacuum ($p < 10^{-10}$ torr). Light from a synchrotron source was incident on the cleaved surface at a 75° angle to the surface normal and largely p-polarized. A double pass cylindrical mirror electron spectrometer with symmetry axis along the sample normal performed the energy analysis of the emitted electrons. Electron Energy Distributions Curves were recorded for photon energies ranging from 7 to 30 eV. The energy resolution in the spectra obtained is believed to be better than 0.2 eV. In a separate experiment, a spectrum of cleaved (110) HgTe was recorded in a similar manner, but using a He discharge with monochromator as light source.

3. RESULTS

The selective breakdown of the VCA is apparent in the photon energy and compositional

* Supported by DARPA Contract No. MDA 903-80-C496 and in part by AFOSR. A portion of this work was performed at the Stanford Synchrotron Radition Laboratory which is supported by the National Science Foundation through the Division of Materials Research.

dependence of the photoemission spectra. Peaks in the emission from the upper, mainly p-like valence states within ~3.5 eV of the VBM shift in binding energy as the photon energy is varied (Figure 1). Such dispersion with hν is characteristic of direct transitions between extended states [9]. As indicated in Figure 1, the emission from the upper portion of the valence bands shows similar features for all compositions.

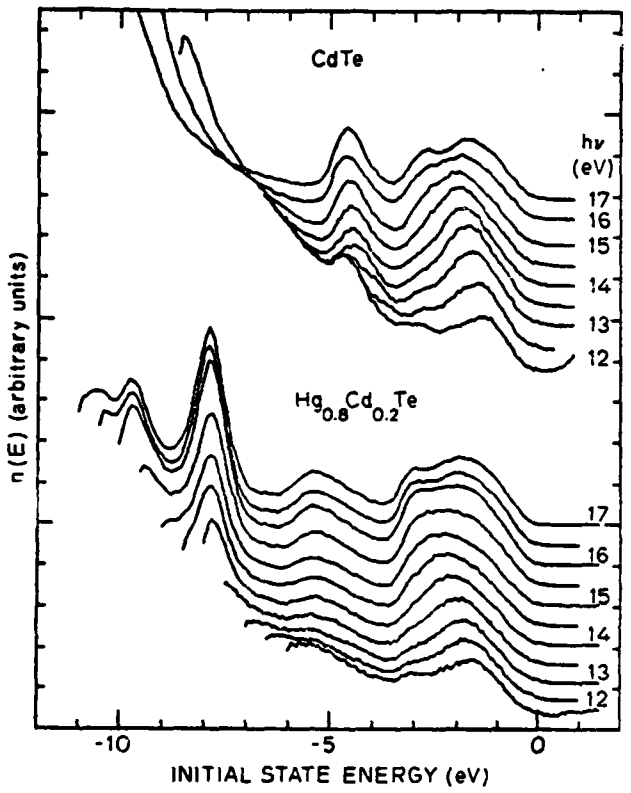

Fig. 1. Photon energy dependence of the valence band emission of $Hg_{1-x}Cd_xTe$

The mainly metal s-electron derived states in the region 4 to 6 eV below the VBM show little or no dispersion with photon energy but exhibit stronger compositional dependence then the upper, p-like bands [8]. The emission from this region is shown in Figure 2, where it is compared to the density of states in this energy range calculated in both the VCA and coherent potential schemes. The experimental and theoretical curves are aligned by superimposing the leading edge of the measured electron distribution with the VBM given by the calculations. Broadening has not been applied to the calculated curves nor background corrections made to the measured ones. As can be seen in the figure, the general experimental features and trends in the alloys are predicted well by the CPA but not by the VCA. In the virtual crystal case, a single sharp peak is predicted which remains sharp and shifts monotomically with decreasing Cd content. The UPS data show instead a broadening of the band as Hg is added and a

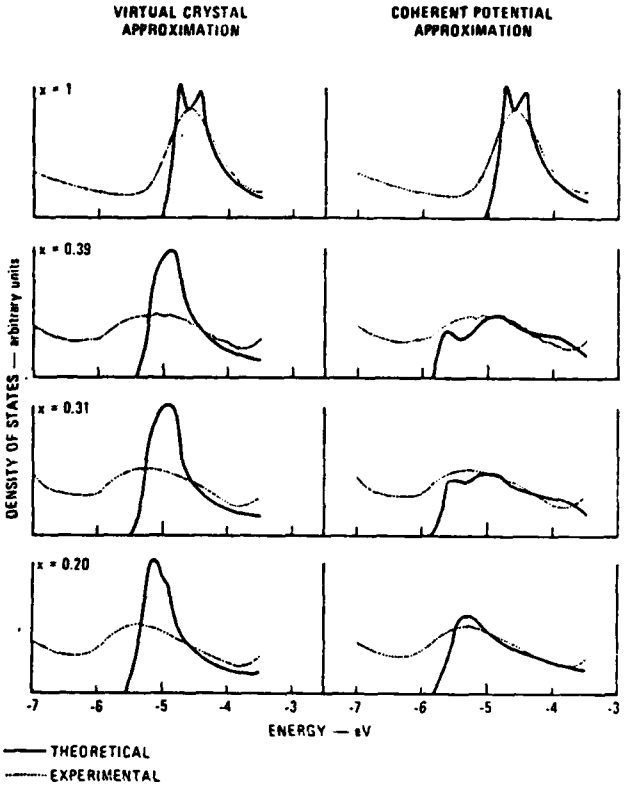

Fig. 2. Comparison of theory and experiment for $Hg_{1-x}Cd_xTe$

decrease in emission near -4.6 eV as the Cd content is reduced. This behavior is reproduced by the structure in the CPA density of states: The peaks at -5.6 and -4.2 eV in the x = 0.31 curve arise from Hg and Cd valence s-electrons, respectively, while the center peak near -5.0 eV is of cation p-character and exhibits VCA-like movement with x.

In addition to the separate contributions of Hg and Cd valence s-electrons to the electronic structure, the differences in Hg-Te and Cd-Te bonds are manifest in the change in binding energy relative to the valence band maximum of the Cd 4d and Hg 5d core levels. Figure 3, showing spectra recorded at 21 eV, details the location of these core levels relative to the VBM for the four samples studied. A spectrum obtained with hν = 21.2 eV from cleaved (110) HgTe is also shown. The peaks at -7.9 and -9.6 eV in the alloy arise from the spin-orbit split Hg 5d levels, while the Cd 4d lines appear around -10.4 eV and are split by 0.6 eV. Apparent in Figure 3 in a shift of 0.2 eV to higher binding energy of the Cd d-levels in going from CdTe to the x = 0.39 alloy and a smaller decrease in binding energy of the Hg 5d lines between HgTe and the alloys. The Cd and Hg contributions to the bonding, therefore, vary as the average composition changes.

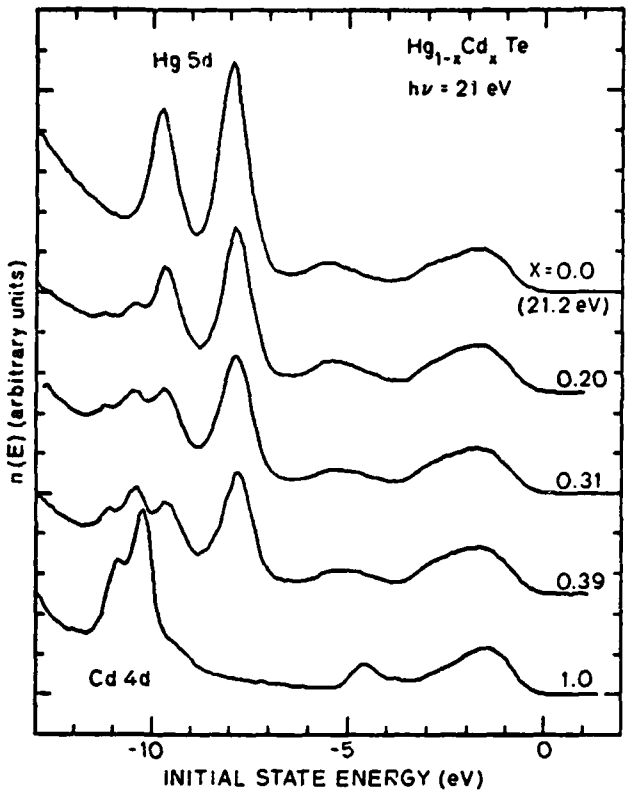

Fig. 3. Comparison of valence band and cation core level emission.

4. DISCUSSION

The breakdown of the VCA as well as the variation in the alloy bandgap are consequences of the difference in cation valence electron s-state energy and can be understood by considering atomic Cd and Hg. The Hg 6s electrons are bound 1.4 eV more strongly than the 5s electrons in Cd [10] while the p-state energies are nearly equal. The increase in binding energy arises from relativistic interactions which more strongly affect s- than p-orbitals and are greater in the higher Z Hg. The role of the cation s-electron in determining the bandgap in the alloy is illustrated by a model calculation of the band structure [1] performed within the VCA where the bands for HgTe were made to approximate those of CdTe by shifting the energy of the cation s-state. That this s-shift arise from relativistic interactions became clear by evaluating the contribution to the calculated energy of the states at the band edge from terms in a relativistic Hamiltonian used in a tight binding calculation of the alloy band structure [3]. Away from the band edges, the difference in cation s-state energy results in separate contributions to the electronic structure and the breakdown of the VCA. Because the Hg valence electrons are more tightly bound, bond formation with Cd may be favored. The shift in energy of the Cd 4d and Hg 5d core lines as the Hg content increases is consistent with this view, with the Cd-Te bond becoming more ionic. A variation in the separation of Hg and Cd d-levels as a function of composition has been observed in HgCd alloys [11]; the explanation of this effect as due to d-band overlap is unlikely to apply to the case of $Hg_{1-x}Cd_xTe$, where the cations are second neighbors. Size effects may also contribute to the reduced Hg-Te bond strength [12].

The ease with which lattice defects are formed and the difficulty of growth of alloys with low Cd content may be a consequence of the increased difference in cation bonding. Because the variation in bandgap and breakdown of the VCA arise from the same feature, the large difference in cation valence electron binding energy, these difficulties will likely occur in other semiconductor alloy systems where the bandgap varies over such a large range.

References

[1] H. Overhof, Phys. Stat. Sol. B45 (1971) 315.

[2] Shin-ichi Katsuki and Makoyo Kunimune, J. Phys. Soc. Jap. 31 (1971) 415.

[3] A. Kisiel and P. M. Lee, J. Phys. F2 (1972) 395.

[4] D. J. Chadi and Marvin L. Cohen, Phys. Rev. B7 (1973) 692.

[5] M. Podgorny and M. T. Czyzyk, Sol. State Comm. 32 (1979) 413.

[6] R.F.C. Farrow, G. R. Jones, G. M. Williams, D. W. Sullivan, W.J.O. Boyle, and J.T.M. Wotherspoon, J. Phys. D12 (1979) L117.

[7] A.-B. Chen and A. Sher, J. Vac. Sci. Tech. 21 (1982) 138.

[8] J. A. Silberman, P. Morgen, I. Lindau, W. E. Spicer and J. A. Wilson, J. Vac. Sci. Tech. 21 (1982) 142.

[9] W. E. Spicer in B. O. Seraphin, Optical Properties of Solids--New Developments (North-Holland, Amsterdam, 1976).

[10] C. E. Moore, Atomic Energy Levles as Derived from analysis of Optical Spectra (U.S. Gov't Printing Office, Washington, D.C., 1958).

[11] J. A. Nicholson, R.C.G. Leckey, J. D. Riley, J. G. Jenkin, and J. Liesgang, J. Phys. F9 (1979) 393.

[12] J. C. Phillips and J. A. Van Vechten, Phys. Rev. B2 (1970) 2147.